DR. MARIA JULIA LAMBERTI (Orcid ID : 0000-0001-7162-0520)

Article type : Research Article

Recapitulation of Hypoxic Tumor-stroma Microenvironment to Study Photodynamic Therapy Implications

María Julia Lamberti[1], Ana Belén Morales Vasconsuelo[1], María Gracia Ferrara[1], Natalia Belén Rumie Vittar[1]

[1] Instituto de Biotecnología Ambiental y Salud (INBIAS), Consejo Nacional de Investigaciones Científicas y Técnicas (CONICET), Departamento de Biología Molecular, Facultad de Ciencias Exactas, Físico-Químicas y Naturales, Universidad Nacional de Río Cuarto, Córdoba, Argentina

*Corresponding author e-mail: belenrumie@gmail.com (Natalia Belén Rumie Vittar)

This article has been accepted for publication and undergone full peer review but has not been through the copyediting, typesetting, pagination and proofreading process, which may lead to differences between this version and the Version of Record. Please cite this article as doi: 10.1111/php.13220

ABSTRACT

Tumor microenvironment (TME) is a dynamic ecosystem where fibroblasts are recruited in order to provide a niche to support growth and, in some extent, to promote therapeutic resistance. However, the role of fibroblasts in stimulating or impairing Photodynamic Therapy (PDT) outcome has not yet been fully addressed. PDT is based on interactions between light, oxygen and photosensitizer, leading to phototoxic reactions that culminate in cell death. In this study, we demonstrated the consequences of a hypoxic stromal phenotype on tumor mass for exploring PDT response. We mimicked TME complexity implementing colon cancer cells and fibroblasts 3D cultures called spheroids. Using hypoxia reporting lines, we verified that homotypic spheroids exhibited a size-dependent transcriptional HIF-1 activity. When co-cultured, fibroblasts were localized in the hypoxic core. In homotypic stromal spheroids, the distribution of the endogenous photosensitizer PpIX was homogeneous while decreased in hypoxic areas of tumor 3D cultures. When monocultured, fibroblasts were more efficient to produce PpIX from its prodrug Me-ALA. Interestingly, the cross-talk between cancer cells and fibroblasts attenuated PpIX accumulation and conferred tumor PDT resistance when compared to homotypic 3D-cultures. Overall, our data suggest that stroma and tumor act in an integrated, reciprocal fashion which could ultimately influence on therapeutic response.

INTRODUCTION

Photodynamic therapy (PDT) is an adjuvant or palliative treatment modality for both non-malignant conditions and malignant neoplasms. In cancer treatment, PDT employs light activation of tumor-localized drug called photosensitizer (PS) in an oxygen-dependent process which initiates oxidative stress. Reactive oxygen species (ROS) finally promote cell death. Thus, efficacy of PDT depends on combined action of three components: PS, light and oxygen (1–4). Dr Thomas Dougherty was the first to report the long-term cures of murine skin tumors after PDT treatment. Given the absence of adverse secondary effects and the minimal damage to overlying skin, this study confirmed the effectiveness and safety of the method (5). Since then, several pre-clinical and clinical researches have been developed and the indication of this treatment for cancer is continuously expanded (6).

Regarding PSs, the photosensitizing properties of endogenous porphyrins have been discovered about 100 years ago. In this context, Protoporphyrin IX (PpIX) is a strong and endogenous PS, which assembles in mitochondria through the heme biosynthetic pathway. Following exogenous administration of 5-aminolevulinic acid (ALA) or its derivatives (e.g. methyl-ALA, here Me-ALA), PpIX accumulates within cells and its excitation by red-light exposure leads to cellular damage (7, 8). The main advantage of PpIX relative to other photosensitizers is the short half-life of its photosensitizing effects (9) and the quite low ~~of~~ levels of circulating PpIX (10).

Even with the improved photosensitizer design and synthesis, and the advanced light delivery technology, hypoxia is still a big dilemma, which makes PDT self-limited. This could be attributed to the native tumor hypoxia and secondary low oxygen saturation caused by PDT itself (11). In hypoxic regions, the transcription factor HIF-1 acts as the main molecular mediator of adaptability. Interestingly, we have previously reported that HIF-1 confers therapeutic resistance to PDT (12).

Overall, oxygen is clearly an important aspect of PDT that should be considered when performing PDT-based clinical and pre-clinical assays. To address this limitation, three dimensional (3D) spheroids models can be advantageous for treatment studies, as many environmental variables can be controlled and adjusted. Spheroid cultures are unique systems that replicate many of the features found within tumors *in vivo*, including deposition of extracellular matrix, cellular polarization, steep oxygen gradients, acidosis, hypoxia and necrotic cores (13, 14).

While many multicellular spheroids are monocultures, co-culture spheroids have seen extensive use and can model aspects of tumor heterogeneity. In this context, tumor microenvironment (TME) is a dynamic evolutionary ecosystem where fibroblasts are recruited in order to provide the niche to support growth (15, 16). As a foundation for developing more reliable pre-clinical models to study photodynamic outcome, our previous experiments have shown the negative impact of the presence of fibroblasts on tumor cell sensitivity to PDT. Moreover, secretome profiling demonstrated that the presence of these stromal cells was associated with HIF-1 pathway exacerbation (17).

Because tumor response to therapy is strongly affected by microenvironmental factors, the use of 3D cultures appears particularly appropriate for the simultaneously study of key cellular parameters that affect drug response and TME biology (14). Given the above, in this study we developed and characterized a hypoxic 3D co-culture of tumor and stromal cells to gain insight into the influence of cellular and non-cellular components of TME on PpIX metabolism and PDT therapeutic response.

MATERIALS AND METHODS

Cell culture. SW480 human colorectal adenocarcinoma and MRC-5 human normal lung fibroblasts were grown, as previously described, "in complete medium DMEM (Dulbecco's modified Eagle medium high glucose 1X, Gibco) supplemented with 10% v/v fetal bovine serum (FBS) (PAA Laboratories), 1% v/v glutamine (GlutaMAXTM 100X Gibco), 1% v/v antibiotic (Penicillin 10,000 units/mL - streptomycin 10,000 μg/mL Gibco) and 1% v/v of sodium pyruvate 100 mM (Gibco). Cells were maintained in 5% CO_2 and 95% air at 37°C in a humidified incubator" (17). SW480 cells

constitutively expressing green fluorescence protein GFP (SW480-G) were generated by stable transfection with pZsGreen1-N1 (Clontech) plasmid (18). SW480 and MRC-5 cells constitutively expressing hypoxia response element fused-GFP (HRE-GFP) construct (SW480-HRE and MRC-5-HRE, respectively) were generated by stable transfection with a plasmid containing the gene for destabilized EGFP placed under the control of a promoter region consisting of five copies of a 35-bp fragment from the HRE of the human VEGF gene and a human cytomegalovirus (CMV) minimal promoter. The plasmid was kindly provided by Dr. Foster (University of Rochester, USA) (12, 19). Transfections were performed using FuGENE® HD Transfection Reagent (Roche) according to manufacturer´s instructions. MRC-5 cells constitutively expressing red fluorescent protein RFP (MRC-5-R) were generated by lentiviral infection of pRFP-LC3 plasmid (17). Generation of recombinant lentivirus was carried out as described previously (20). SW480-G, SW480-HRE and MRC-5-HRE stable transfected cells were selected in growth medium supplemented with 2 mg/ml of active Geneticin (G418) (Life Technologies). Individual colonies were isolated after 2–3 weeks of growth under selection using the cloning ring method and subsequently expanded into clonal cell lines. Expression of GFP or RFP was assessed by fluorescence microscope (18).

Three dimensional cultures (3D) generation. Homotypic (100% tumor cells or 100% fibroblasts) and heterotypic (50% tumor cell + 50% fibroblasts) spheroids were generated using liquid overlay technique, as previously described (21). Briefly, an agarose stock solution (1%) was prepared in H_2O and sterilized by autoclaving. Prior to seeding of the cells, bottoms of 96-well plates were coated with agarose. After cooling for 0.5 h, the plates were ready to use. Cell suspensions were prepared, allowing the seeding of the desired cellular concentration in a total volume of 100 μL. Using this protocol, after 72 h, spheroids were generated with a homogeneous size distribution of similar diameter.

Hypoxia reporter assays - Fluorescence imaging. For fluorescence quantification experiments, SW480-HRE or MRC-5-HRE homotypic spheroids (2000, 5000, 10000 and 20000 cells/spheroid) were imaged using an inverted Carl Zeiss fluorescence microscope coupled to a high resolution monochromatic digital camera at 10× magnification. For GFP visualization, Nikon B-2A fluorescence

filter was used (excitation filter: 470/40 nm). Exposure times were kept constant during experiments. For GFP imaging, background signal was subtracted using specific algorithm from ImageJ software (1.46r version), and brightness was adjusted. All image corrections were kept similar within experiments. Regions of interest were manually drawn for each spheroid, and areas were quantified. Hypoxic (GFP +) and non-hypoxic (GFP -) zones were identified and graphically represented as a percentage of total spheroid area.

Characterization of spheroids morphology. The morphology of homotypic (100% SW480-G or 100% MRC-5-R) and heterotypic (500% SW480-G + 50% MRC-5-R) spheroids (20000 cells/spheroid) was assessed by fluorescence microscopy using an inverted Carl Zeiss fluorescence microscope coupled to a high resolution monochromatic digital camera at 10× magnification. For GFP visualization, Nikon B-2A fluorescence filter was used (excitation filter: 470/40 nm). For RFP visualization, Nikon G-2A fluorescence filter was used (excitation filter: 535/50 nm). As mentioned above, SW480-G tumor cells constitutively expressed GFP and MRC-5-R fibroblasts cells constitutively expressed RFP. The size of the spheroids was analyzed using the calibration analysis tools of the ImageJ software (1.46r version). ImageJ Plot Profile tool was used to measure the distribution of fibroblast RFP and tumor GFP signal intensities along the spheroid longitudinal diameter (900 μm line).

Visualization and measurement of the photosensitizer PpIX. Homotypic (100% SW480 or 100% MRC-5) and heterotypic (500% SW480 + 50% MRC-5) spheroids (20000 cells/spheroid) were transferred from agarose-coated plates to plates without agarose and washed twice with PBS to remove all traces of FBS and then incubated with Me-ALA (0-1 mM, Sigma) in growth medium without FBS for 24 h. PpIX generation was assessed by fluorescence imaging and flow cytometry.

Fluorescence imaging for PpIX spatial distribution analysis. For PpIX spatial distribution analysis, homotypic and heterotypic spheroids were imaged using an inverted Carl Zeiss fluorescence microscope coupled to a high resolution monochromatic digital camera at 10× magnification. For PpIX visualization, Nikon G-2A fluorescence filter was used (excitation filter: 535/50 nm). Exposure

times were kept constant during experiments. For PpIX imaging (red fluorescence), background signal was subtracted using specific algorithm from ImageJ software (1.46r version), and brightness was adjusted. All image corrections were kept similar within experiments. Regions of interest were manually drawn for each spheroid (whole spheroid), fluorescence mean was quantified and expressed as PpIX intensity. ImageJ Plot Profile tool was used to measure the distribution of PpIX signal intensity along the spheroid longitudinal diameter (900 µm line).

Flow cytometry for PpIX emission measures. Spheroids were trypsinized, centrifugated for 5 min at 2000 rpm, washed twice with PBS and finally resuspended in PBS. PpIX emission measures were collected employing Millipore Guava Easycyte 6 2L flow cytometer and analyzed by FlowJo 10.0.7 software (22).

Photodynamic treatment. Homotypic (100% SW480-G or 100% MRC-5-R) and heterotypic (500% SW480-G + 50% MRC-5-R) spheroids (20000 cells/spheroid) were transferred from agarose-coated plates to plates without agarose and washed twice with PBS before Me-ALA (0.2 mM) addition during 24 h in growth medium without FBS. After Me-ALA incubation, spheroids were irradiated at room temperature with monochromatic light source (636 nm ± 17 nm) using a MultiLED system (dose: 50.4 J/cm^2). The fluence rate was 28 mW/cm^2. Finally, the drug solution was removed and replaced with fresh complete medium (17)

Viable tumor cell counting. Twenty-four hour after photodynamic treatment, spheroids were disaggregated by trypsinization and cells were centrifuged, resuspended in PBS and loaded into each chamber of the hemocytometer. Counts were performed under a 40× objective according to the standard methodology (23). For GFP visualization, Nikon B-2A fluorescence filter was used (excitation filter: 470/40 nm). For RFP visualization, Nikon G-2A fluorescence filter was used (excitation filter: 535/50 nm). The results were expressed as the percentage of viable tumor GFP + and/or fibroblast RFP + cells in relation to the counts obtained on untreated spheroids.

Statistical analysis. Differences between groups were tested by 1 or 2-way analysis of variance with

Bonferroni post-hoc tests using GraphPad Prism 7 software. All the results are expressed as mean ± standard error of at least three independent experiments, and $P<0.05$ was considered statistically significant. References of figures: $P<0.05$ = *; $P<0.01$ = **; $P<0.001$ = ***; $P<0.0001$ = ****.

RESULTS

Impact of spheroids hypoxia on tumor and stromal distribution

We have previously demonstrated that SW480-HRE spheroids of ~900 µm diameter exhibited a basal hypoxia and showed a radial increase in hypoxic areas from the periphery towards the center (12). However, there is no evidence in the literature regarding hypoxic core development in stromal homotypic 3D cultures. In this study, we used hypoxia reporter cell lines (tumor SW480-HRE and fibroblasts MRC-5-HRE) that stably express GFP under the control of an HRE element containing the DNA binding motif for the hypoxia inducible transcription factor HIF-1. Thus, GFP positive (GFP+) regions represented hypoxic layers wherein HIF-1 was transcriptionally activated (12). Liquid overlay technique was applied in order to generate spheroids with homogeneous size distribution dependent on cell seeding concentration. In these conditions, tumor and stromal cells formed one centrally positioned spheroid in each well of the U-bottom of agarose-coated 96-well plates when cultured for 3 days (Figure 1A-B). Spheroid size appeared to be associated with HIF-1 induction (Figure 1C-D), progressing from normoxic cells at the periphery to hypoxic cells at the center (Figure 1A-B). Surprisingly, compared to tumor spheroids, fibroblasts 3D-structures developed higher GFP+/GFP– ratio, in all cell seeding concentration tested (Figure 1). As representative of tumor microenvironment hypoxia, for the next experiments, we focused on 20000 initial cells/spheroid, which displayed a 56.7±2.9% and 81.8±14.2% of HIF transcriptional activity (GFP+ cells), regarding low oxygen area, in tumor and stromal 3D cultures, respectively.

<Figure 1>

Architecture of tumor-stroma hypoxic co-culture

It is well-known that hypoxia influences the behavior of tumor and stromal cells. In this sense, we asked whether this key microenvironmental factor can affect 3D-cultures architecture. Tumor SW480-G cells, constitutively expressing GFP, and fibroblasts MRC-5-R cells, constitutively expressing RFP (17), at a seeding density of 20000 cells/spheroid, were cultured alone (homotypic spheroids) or as a 1:1 mixed suspension (heterotypic spheroids) in U-bottom agarose-coated 96-well plates. Morphology of spheroids was monitored according to size and populations distribution at day 3 (Figure 2A). SW480-G and MRC-5-R cells formed spheroids of 952.2±22.15 and 565.1±35.1 μm in diameter, respectively (Figure 2B). In concordance with our previous results (17), compared to homotypic tumor spheroid, the presence of fibroblasts reduced the diameter of the whole spheroids (Figure 2B). When different cell lines are co-cultured in a 3D model, spheroids may either distinguish as mosaics of mixed cells or, alternatively, as hybrid spheroids with incomplete mixing of the cell types (24). Fluorescence tracking of tumor and stromal cells in 3D mixed-cell spheroids demonstrated a hybrid distribution of both types of cells (Figure 2A). Surprisingly, relative localization of fibroblasts cells in the central region was observed (Figure 2A and 2C), which suggested a preferential hypoxic accumulation of stroma in this avascular *in vitro* tumor microenvironment.

<Figure 2>

Endogenous PpIX generation in stromal and tumor 3D cultures

The spatial patterns of therapeutic efficacy can result from a host of factors, including the uptake and localization of PS. Although most PSs are exogenously administered drugs, PpIX is an effective endogenous PS generated following excess administration of ALA or its derivatives (9, 25). We have previously demonstrated that, for colorectal cancer spheroids, the ideal experimental design included the application of the Me-ALA prodrug during 24 h in order to allow PpIX generation (12). By using the same protocol, we aimed here to characterize the hypoxic stromal or tumor metabolism of Me-ALA to the active photosensitizer PpIX. Homotypic SW480 or MRC-5 spheroids, at a seeding density

of 20000 cells/spheroid, were grown for 3 days and then incubated with increasing concentrations of the prodrug for 24 h. Epifluorescence live microscopy (Figure 3A and 3B) and flow cytometry (Figure 3C and 3D) data demonstrated that tumor PpIX generation was Me-ALA dose-dependent. We have reported that normoxic SW480 colorectal cancer cells were able to produce higher PpIX compared to normoxic MRC-5 fibroblasts (17). On the opposite, here we observed an enhanced stromal PpIX generation (Figure 3B), suggesting that hypoxia could be a key factor modulating this endogenous PS metabolism.

<Figure 3>

Stromal influence on PpIX generation in hypoxic heterotypic spheroids

Considering the results described above, here we investigated PpIX differential generation between tumor-stromal monospheroids *vs* co-cultured spheroids. At low Me-ALA concentration (0.2 μM), in concordance with our previous results (12), tumor spheroid exhibited a decreased PS generation from the periphery towards the center, whereas the distribution of PpIX was homogeneous in stromal spheroids (Figure 4A and 4B). Surprisingly, photosensitizer production was significantly inhibited in mixed spheroids (Figure 4A and 4B). To identify the impact of PDT on homo and heterotypic spheroids, Me-ALA incubated 3D-cultures were exposed to red-light irradiation. They were disaggregated 24 hours after photosensitization and viable GFP + tumor cells and viable RFP + fibroblasts were quantified. Fibroblasts 3D-cultures did not exhibit a preferential sensitivity to photodynamic treatment when compared to their tumor counterpart (Figure 4C, Table 1). Interestingly, the presence of fibroblasts increased heterotypic spheroid photoresistance (Figure 4C, Table I). These data suggest that the cross-talk between cancer cells and fibroblasts within heterotypic spheroids affect both PpIX metabolism and PDT outcome.

<Figure 4>

<Table 1>

DISCUSSION

The concept of the tumor microenvironment (TME) encompasses both the stromal components and the cancer cells (26). It is well known that stroma contributes to the majority of the hallmark capabilities of tumor cells, and directly determines clinical outcomes (27). During TME development and progression, cellular populations are often limited to enough nutrients and oxygen supply. Thus, most solid tumors develop hypoxia areas wherein hypoxia-inducible factors (HIFs) are actively expressed. HIF-dependent signaling can promote the adaptation and selection of both cancer and stromal cells to the surrounding conditions, ultimately leading to cancer progression (28). Fibroblasts are considered the main critical stromal cell population that secrete proliferative and pro-metastatic growth factors involved in cancer progression and contribute to the generation of a drug resistant environment (29). Given the above, in this article, we aimed to describe the influence of hypoxia on tumor and fibroblasts ecosystem and how impact on anticancer therapeutic response.

In order to replicate TME inherent architecture *in vitro*, a spheroid model was used. In both tumor and stromal 3D cultures, we observed the generation of a hypoxic environment and activation of its main effector, HIF-1. Interestingly, even being smaller, fibroblasts spheroids developed higher hypoxic areas than their tumor counterparts (Figure 1). Physical and chemical composition of extracellular matrix (30), cellular metabolism rate (31, 32) and differentiation status (31, 32) are 3D-culture´s characteristics that have been associated to non-uniform oxygen consumption or oxygen diffusion properties. Furthermore, the presence of fibroblasts-like cells in tumor spheroids increased the expression of ECM proteins (33). Further studies should be done to deeply describe the relevance of these features in our experimental model.

In addition to the impact on tumor cell biology, the influence that hypoxia exerts on the surrounding cells represents a critical step in the tumorigenic process. Here, we have provided unique insights into stromal and tumor cell responses to hypoxia by performing heterologous spheroid culture in which

tumor cells (SW480) were combined with fibroblasts (MRC-5) during the sphere forming procedure. In concordance with previous studies (33–35), cells were spatially segregated, ~~and~~ resulting in localization of stromal cells in the central core hypoxic regions of 3D co-culture sphere (Figure 2). In this sense, the link between hypoxia and fibroblasts has been previously introduced by us when demonstrating that HIF-1 pathway was enriched in secretome of hypoxic microtumors that co-exist with fibroblasts cells in a 3D environment (17). These data agree with an earlier report that showed the ability of the TME to induce a hypoxia-related phenotype particularly in stromal cells of host origin (36).

In addition to prompting an aggressive phenotype, tumor hypoxia presents several challenges to therapeutic intervention (37). One particular issue is Photodynamic Therapy (PDT), in which hypoxic environment not only renders tumor cells privileged or resistant to the photo-intervention, but also involves the limitation of one of its main active factors: the oxygen (16). As mentioned above, PDT employs a combination of photosensitizer, light, and molecular oxygen, to selectively exert oxidative stress-related cytotoxic activity on target cells (1–4). In addition, previous reports have demonstrated that low oxygen pressure affects the prodrug ALA metabolism towards the photosensitizer PpIX generation via heme pathway (38, 39). Specifically, hypoxia up-regulates the expression of enzymes ferrochelatase (40) and heme oxygenase (41), suggesting an increased ability for the conversion of PpIX into photoinactive heme. We have demonstrated that inhibiting HIF-1 in tumor spheroids increased PpIX (12). In this study, the mini-TME 3D model had significant potential for studying the hypoxic response of tumor and stromal cells following PDT and the specific mechanisms used to circumvent this treatment, i.e. endogenous PS metabolism. Regarding this hypothesis, we have demonstrated that 20000 cells initial-seeding stromal spheroids exhibited a higher PpIX content compared to their tumor counterpart (Figure 3). Several explanations can be proposed for the observed patterns of endogenous photosensitizer generation. Firstly, the smaller size of the fibroblast 3D culture (Figure 2B) could facilitate the homogeneous prodrug Me-ALA penetration and conversion, and this could be partially linked to the PpIX gradient developed in tumor spheroids (Figure 3A). On the other hand, it has been demonstrated that PpIX accumulation revealed a positive relationship with cell dormancy, which is characterized by no proliferation but no cell death (42). Here, we observed that

fibroblasts had lower proliferation rate than tumor cells when grown as spheroids (Table 1), which suggest a dormancy status that could in part explain the enhanced PpIX stromal generation. Overall, further research on cell selectivity of PpIX fluorescence enhancement should focus on the mechanisms responsible for an altered PpIX metabolism to find stromal population-specific target molecules, thus leading to an improved clinical practicability of Me-ALA application on TME component disruption.

Given that cancer-associated fibroblasts are strongly implicated in tumor progression, the targeting of them using various therapeutic approaches is a novel treatment strategy. Based on our results, we initially proposed 0.2 mM Me-ALA as fibroblast-targeting concentration of prodrug. This experimental design was selected given that, under these conditions, PpIX was significantly incremented in fibroblasts spheroids whereas remained almost basal in tumor spheroids (Figure 3). Unexpectedly, tumor-fibroblast crosstalk within hypoxic environmental conditions negatively affected PpIX generation (Figure 4A and 4B), which supports the idea that stromal cells functional and physical interact with each other and with the cancer cells in a dynamic and context dependent manner (26). In this scenario, the juxtacrine and/or paracrine signaling stablished between hypoxic coexisting tumor and fibroblasts could influence PpIX associated metabolism, conversion or efflux enzymes which ultimately lead to an overall decrease in PS availability. The inclusion of multiple cell types in the heterotypic spheroid model makes it difficult to determine the influence of a specific cell population on this response. Nonetheless, this result could partially explain why the presence of fibroblast cells reduced the cytotoxic effect of PDT towards tumor cells when compared to homotypic 3D-cultures (Figure 4C and Table 1).

Here, we have constructed a complex culture models that recapitulate aspects of the *in vivo* tumor microenvironment to study the dynamics of tumor development and therapy. In concordance to previous studies, this *in vitro* tumor modelling can be further applied to the study of several cancer hallmarks (e.g., cell proliferation, metastasis, metabolism) in an avascular tumor microenvironment, drug screening, tumor angiogenesis, tumor–immune cell interactions, among others (43).

In conclusion, our data suggest that stroma and tumor act in an integrated, reciprocal fashion which could ultimately influence on PDT resistance. Therefore, mimic tumor biology complexity is relevant to optimize PDT efficacy due to the coexisting cells behavior differ that isolated populations.

ACKNOWLEDGMENTS*:* This work was supported by grants from Consejo Nacional de Investigaciones Científicas y Técnicas (PIP-CONICET), Agencia Nacional de Promoción Científica y Tecnológica (PICT), Secretaría de Ciencia y Técnica (PPI-SECyT), Universidad Nacional de Río Cuarto (UNRC), Argentina. NBRV is member of the Scientific Researcher Career at CONICET and professor at UNRC. MJL hold postgraduate fellowship from CONICET. ABMV hold graduate fellowship from CONICET. MGF hold undergraduate fellowship from CIN.

REFERENCES

1. Dougherty, T. (2010) Introduction. *Methods Mol Biol.* **635**, 1–6.

2. Milla Sanabria, L., Rodríguez, M., Cogno, I., Rumie Vittar, N., Pansa, M., Lamberti, M. and Rivarola, V. (2013) Direct and indirect photodynamic therapy effects on the cellular and molecular components of the tumor microenvironment. *Biochim Biophys Acta.* **1835**, 36–45.

3. Dougherty, T. (2002) An update on photodynamic therapy applications. *J Clin Laser Med Surg.* **20**, 3–7.

4. Rivarola, V. A., Rumie Vittar, N. B., Lamberti, M. J., Sanabria, L. M., Pansa, M. F., Fernández, I. M., Cogno, I. S. and Rodríguez, M. E. (2013) Cell death and resistance mechanisms triggered by photodynamic therapy. In *Photodynamic Therapy: New Research*, pp. 187–230.

5. Dougherty, T., Grindey, G., Fiel, R., Weishaupt, K. and Boyle, D. (1975) Photoradiation therapy. II. Cure of animal tumors with hematoporphyrin and light. *J Natl Cancer Inst.* **55**, 115–121.

6. Agostinis, P., Berg, K., Cengel, K., Foster, T., Girotti, A., Gollnick, S., Hahn, S., Hamblin, M., Juzeniene, A., Kessel, D., Korbelik, M., Moan, J., Mroz, P., Nowis, D., Piette, J., Wilson, B. and Golab, J. (2011) Photodynamic therapy of cancer: an update. *CA Cancer J Clin.* **61**, 250–281.

7. Brunner, H., Hausmann, F., Krieg, R. C., Endlicher, E., Schölmerich, J., Knuechel, R. and Messmann, H. (2001) The effects of 5-aminolevulinic acid esters on protoporphyrin IX production in human adenocarcinoma cell lines. *Photochem Photobiol.* **74**, 721–725.

8. Wachowska, M., Muchowicz, A., Firczuk, M., Gabrysiak, M., Winiarska, M., Wańczyk, M., Bojarczuk, K. and Golab, J. (2011) Aminolevulinic acid (ALA) as a prodrug in photodynamic therapy of cancer. *Molecules* **16**, 4140–4164.

9. Casas, A., Fukuda, H., Di Venosa, G. and Batlle, A. (2001) Photosensitization and mechanism of cytotoxicity induced by the use of ALA derivatives in photodynamic therapy. *Br J Cancer.* **85**, 279–284.

10. Bellnier, D., Greco, W., Loewen, G., Nava, H., Oseroff, A. and Dougherty, T. (2006) Clinical pharmacokinetics of the PDT photosensitizers porfimer sodium (Photofrin), 2-[1-hexyloxyethyl]-2-devinyl pyropheophorbide-a (Photochlor) and 5-ALA-induced protoporphyrin IX. *Lasers Surg Med.* **38**, 439–444.

11. Agostinis, P., Berg, K., Cengel, K. ., Foster, T. ., Girotti, A. ., Gollnick, S. ., Hahn, S. ., Hamblin, M. ., Juzeniene, A., Kessel, D., Koberlik, M., Moan, J., Mroz, P., Nowis, D., Piette, J., Wilson, B. and Golab, J. (2011) Photodynamic Terapy of cancer: an update. *CA Cancer J Clin.* **61**, 250–281.

12. Lamberti, M., Pansa, M., Vera, R., Fernandez-Zapico, M., Rumie Vittar, N. and Rivarola, V. (2017) Transcriptional activation of HIF-1 by a ROS-ERK axis underlies the resistance to photodynamic therapy. *PLoS One* **12**, e0177801.

13. Vera, R., Lamberti, M., Rivarola, V. and Rumie Vittar, N. (2015) Developing strategies to predict photodynamic therapy outcome: the role of melanoma microenvironment. *Tumour Biol.* **36**, 9127–9136.

14. Hirschhaeuser, F., Menne, H., Dittfeld, C., West, J., Mueller-Klieser, W. and Kunz-Schughart, L. a (2010) Multicellular tumor spheroids: an underestimated tool is catching up again. *J Biotechnol.* **148**, 3–15.

15. Wu, T. and Dai, Y. (2017) Tumor microenvironment and therapeutic response. *Cancer Lett.* **387**, 61–68.

16. Rumie Vittar, N., Lamberti, M., Pansa, M., Vera, R., Rodriguez, M., Cogno, I., Milla Sanabria, L. and Rivarola, V. (2013) Ecological photodynamic therapy: new trend to disrupt the intricate networks within tumor ecosystem. *Biochim Biophys Acta.* **1835**, 86–89.

17. Lamberti, M., Rettel, M., Krijgsveld, J., Rivarola, V. and Rumie Vittar, N. (2019) Secretome profiling of heterotypic spheroids suggests a role of fibroblasts in HIF-1 pathway modulation and colorectal cancer photodynamic resistance. *Cell Oncol (Dordr).* **42**, 173–196.

18. Pansa, M., Lamberti, M., Cogno, I., Correa, S., Rumie Vittar, N. and Rivarola, V. (2016) Contribution of resident and recruited macrophages to the photodynamic intervention of colorectal tumor microenvironment. *Tumour Biol.* **37**, 541–552.

19. Mitra, S., Cassar, S. E., Niles, D. J., Puskas, J. a, Frelinger, J. G. and Foster, T. H. (2006) Photodynamic therapy mediates the oxygen-independent activation of hypoxia-inducible factor 1alpha. *Mol Cancer Ther* **5**, 3268–3274.

20. Brockmeier, U., Platzek, C., Schneider, K., Patak, P., Bernardini, A., Fandrey, J. and Metzen, E. (2011) The function of hypoxia-inducible factor (HIF) is independent of the endoplasmic reticulum protein OS-9. *PLoS One* **6**, e19151.

21. Lamberti, M., Pansa, M., Vera, R., Rumie Vittar, N. and Rivarola, V. (2014) Photodynamic therapy potentiates the paracrine endothelial stimulation by colorectal cancer. *Laser Phys.* **24**, 8.

22. Milla, L., Cogno, I., Rodríguez, M., Sanz-Rodríguez, F., Zamarrón, A., Gilaberte, Y., Carrasco, E., Rivarola, V. and Juarranz, A. (2011) Isolation and characterization of squamous carcinoma cells

resistant to photodynamic therapy. *J Cell Biochem* **112**, 2266–2278.

23. Strober, W. (2001) Trypan blue exclusion test of cell viability. *Curr Protoc Immunol.* **Appendix 3**.

24. Koumenis, C., Coussens, L., Giaccia, A. and Hammond, E. (2016) Tumor Microenvironment: Study Protocols. Springe (Vol. 899).

25. Donnelly, R., McCarron, P. and Woolfson, A. (2008) Derivatives of 5-aminolevulinic Acid for photodynamic therapy. *Perspect Med. Chem* **1**, 49–63.

26. Alkasalias, T., Moyano-Galceran, L., Arsenian-Henriksson, M. and Lehti, K. (2018) Fibroblasts in the Tumor Microenvironment: Shield or Spear? *Int J Mol Sci. 2018 May 21;19(5).* 5.

27. Hanahan, D. and Coussens, L. M. (2012) Accessories to the Crime: Functions of Cells Recruited to the Tumor Microenvironment. *Cancer Cell* **21**, 309–322. https://doi.org/10.1016/j.ccr.2012.02.022.

28. Petrova, V., Annicchiarico-Petruzzelli, M., Melino, G. and Amelio, I. (2018) The hypoxic tumour microenvironment. *Oncogenesis.* **7**, 10.

29. Cirri, P. and Chiarugi, P. (2012) Cancer-associated-fibroblasts and tumour cells: a diabolic liaison driving cancer progression. *Cancer Metastasis Rev* **31**, 195–208.

30. Androjna, C., Gatica, J., Belovich, J. and Derwin, K. (2008) Oxygen diffusion through natural extracellular matrices: implications for estimating 'critical thickness' values in tendon tissue engineering. *Tissue Eng Part A.* **14**, 559–569.

31. Sutherland, R., Sordat, B., Bamat, J., Gabbert, H., Bourrat, B. and Mueller-Klieser, W. (1986) Oxygenation and differentiation in multicellular spheroids of human colon carcinoma. *Cancer Res.* **46**, 5320–5329.

32. Mueller-Klieser, W. (1984) Method for the determination of oxygen consumption rates and diffusion coefficients in multicellular spheroids. *Biophys J.* **46**, 343–348.

33. Song, Y., Kim, S., Kim, K., Choi, E., Kim, J. and Seo, H. (2016) Activated hepatic stellate cells play pivotal roles in hepatocellular carcinoma cell chemoresistance and migration in multicellular tumor spheroids. *Sci Rep.* **6**, 36750.

34. Khawar, I., Park, J., Jung, E., Lee, M., Chang, S. and Kuh, H. (2018) Three Dimensional Mixed-Cell Spheroids Mimic Stroma-Mediated Chemoresistance and Invasive Migration in hepatocellular carcinoma. *Neoplasia.* **20**, 800–812.

35. Yip, D. and Cho, C. (2013) A multicellular 3D heterospheroid model of liver tumor and stromal cells in collagen gel for anti-cancer drug testing. *Biochem Biophys Res Commun.* **433**, 327–332.

36. Fukumura, D., Xavier, R., Sugiura, T., Chen, Y., Park, E., Lu, N., Selig, M., Nielsen, G., Taksir, T., Jain, R. and Seed, B. (1998) Tumor induction of VEGF promoter activity in stromal cells. *Cell.* **94**, 715–725.

37. Rohwer, N. and Cramer, T. (2011) Hypoxia-mediated drug resistance: novel insights on the functional interaction of HIFs and cell death pathways. *Drug Resist Updat* **14**, 191–201. https://doi.org/10.1016/j.drup.2011.03.001.

38. McNicholas, K., MacGregor, M. and Gleadle, J. (2019) In order for the light to shine so brightly, the darkness must be present-why do cancers fluoresce with 5-aminolaevulinic acid? *Br J Cancer*.

39. Wyld, L., Reed, M. and Brown, N. (1998) The influence of hypoxia and pH on aminolaevulinic acid-induced photodynamic therapy in bladder cancer cells in vitro. *Br J Cancer* **77**, 1621–1627.

40. Liu, Y., Ang, S., Weigent, D., Prchal, J. and Bloomer, J. (2004) Regulation of ferrochelatase gene expression by hypoxia. *Life Sci.* **75**, 2035–2043.

41. Lee, P., Jiang, B., Chin, B., Iyer, N., Alam, J., Semenza, G. and Choi, A. (1997) Hypoxia-inducible factor-1 mediates transcriptional activation of the heme oxygenase-1 gene in response to hypoxia. *J Biol Chem.* **272**, 5375–5381.

42. Nakayama, T., Otsuka, S., Kobayashi, T., Okajima, H., Matsumoto, K., Hagiya, Y., Inoue, K., Shuin, T., Nakajima, M., Tanaka, T. and Ogura, S. (2016) Dormant cancer cells accumulate high protoporphyrin IX levels and are sensitive to 5-aminolevulinic acid-based photodynamic therapy. *Sci Rep.* **6**, 36478.

43. Katt, M., Placone, A., Wong, A., Xu, Z. and Searson, P. (2016) In Vitro Tumor Models: Advantages, Disadvantages, Variables, and Selecting the Right Platform. *Front Bioeng Biotechnol.* **4**, 12.

TABLE

Table 1. Number of tumor and fibroblasts counting cells on untreated (control) or PDT-treated (PDT) homotypic and heterotypic spheroids. Twenty-four hour after photodynamic treatment, spheroids were disaggregated by trypsinization and cells were centrifuged, resuspended in PBS and loaded into each chamber of the hemocytometer. Viable tumor GFP+ and/or fibroblast RFP+ cells were counted under a 40× objective according to the standard methodology.

Condition	Spheroid	Tumor GFP+ (cells/ml x 10^6)	Fibroblast RFP+ (cells/ml x 10^6)
Control	*Tumor homotypic*	6.165±0.111	0
	Stromal homotypic	0	2.542±0.281
	Heterotypic	2.805±0.484	1.120±0.374
PDT	*Tumor homotypic*	1.570±0.140	0
	Stromal homotypic	0	0.908±0.194
	Heterotypic	1.860±0.258	0.785±0.252

FIGURE CAPTIONS

Figure 1. Tumor and stroma spheroids develop a size-dependent HIF + hypoxic core

SW480-HRE cancer cells (A-C) or MRC-5-HRE fibroblasts (B-D) were seeded at the concentrations shown (2000, 5000, 10000 and 20000 cells/well) in agarose-coated U-bottom 96 well plates and incubated for 72 hours. (A-B) Representative epifluorescence microscopy images of spheroids. GFP + areas represented where hypoxia where HIF is active. Bar = 100 μm. (C-D) Hypoxic (GFP +) and non-hypoxic (GFP -) areas were quantified and graphically represented as a percentage of total spheroid area.

Figure 2. Preferential stromal distribution of fibroblasts toward hypoxic areas in 3D-co-culture spheroids.

Homotypic (100% SW480-G or 100% MRC-5-R) and heterotypic (50% SW480-G + 50% MRC-5-R) spheroids were seeded at a density of 20000 cells/well in agarose-coated U-bottom 96 well plates and incubated for 72 hours. (A) Representative epifluorescence microscopy images of spheroids. GFP represented tumor cells and RFP represented fibroblasts. Bar = 100 μm. (B) Homotypic and heterotypic spheroid diameters were quantified using the calibration analysis tools of the ImageJ software. (C) The distribution of fibroblast RFP signal and tumor GFP signal intensities along the spheroid longitudinal diameter was evaluated using ImageJ Plot Profile tool.

Figure 3. Endogenous PpIX generation in stromal and tumor 3D cultures

Homotypic (100% SW480 or 100% MRC-5) spheroids were seeded at a density of 20000 cells/well in agarose-coated U-bottom 96 well plates and incubated for 72 hours. Then, they were transferred from agarose-coated plates to plates without agarose and washed twice with PBS to remove all traces of FBS and then incubated with Me-ALA (0-1 mM, Sigma) in growth medium without FBS for 24 h. (A) Representative epifluorescence microscopy images of spheroids incubated with Me-ALA. PpIX shows red fluorescence. (B) Fluorescence mean was quantified within the whole spheroid and expressed as PpIX intensity (au = arbitrary unite). ***$p<0.001$, ****$p<0.0001$, Two-Way ANOVA Bonferroni posttest. (C-D) Representative flow cytometry histograms of PpIX emission measures in tumor (C) and fibroblast (D) homotypic spheroids incubated with Me-ALA. Numbers in parenthesis indicate the percentage of PpIX + cells in each condition.

Figure 4. Fibroblast impact on endogenous PpIX generation and PDT outcome in heterotypic 3D cultures

Homotypic (100% SW480 or 100% MRC-5) and heterotypic (500% SW480-G + 50% MRC-5-R) spheroids were seeded at a density of 20000 cells/well in agarose-coated U-bottom 96 well plates and incubated for 72 hours. Then, they were transferred from agarose-coated plates to plates without agarose and washed twice with PBS to remove all traces of FBS and then incubated with Me-ALA (0.2 mM, Sigma) in growth medium without FBS for 24 h. (A) Representative epifluorescence microscopy images of spheroids incubated with Me-ALA. PpIX shows red fluorescence. (B) The distribution of PpIX signal intensity along homotypic and heterotypic spheroid longitudinal diameter was evaluated using ImageJ Plot Profile tool. (C) Me-ALA-incubated spheroids were exposed to irradiation (50.4 J/cm^2). Viable tumor GFP+ and/or fibroblast RFP+ cells were counted using a hemocytometer and referred to the counts obtained on untreated spheroids (dotted line: 100% viability).

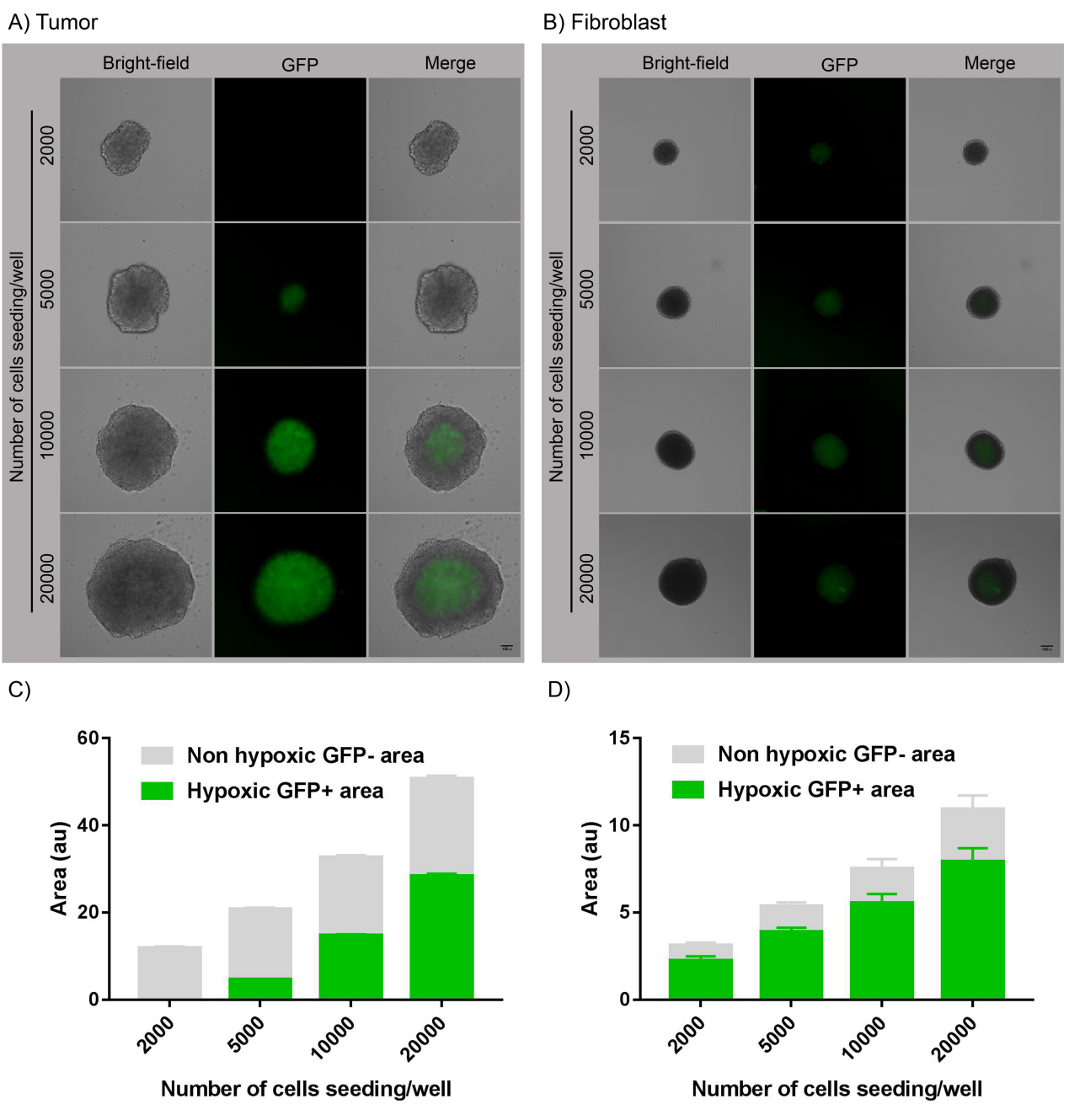
A) Tumor
B) Fibroblast
Bright-field
GFP
Merge
Number of cells seeding/well
2000
5000
10000
20000
C)
D)
Non hypoxic GFP- area
Hypoxic GFP+ area
Area (au)
60
40
20
0
15
10
5
Number of cells seeding/well

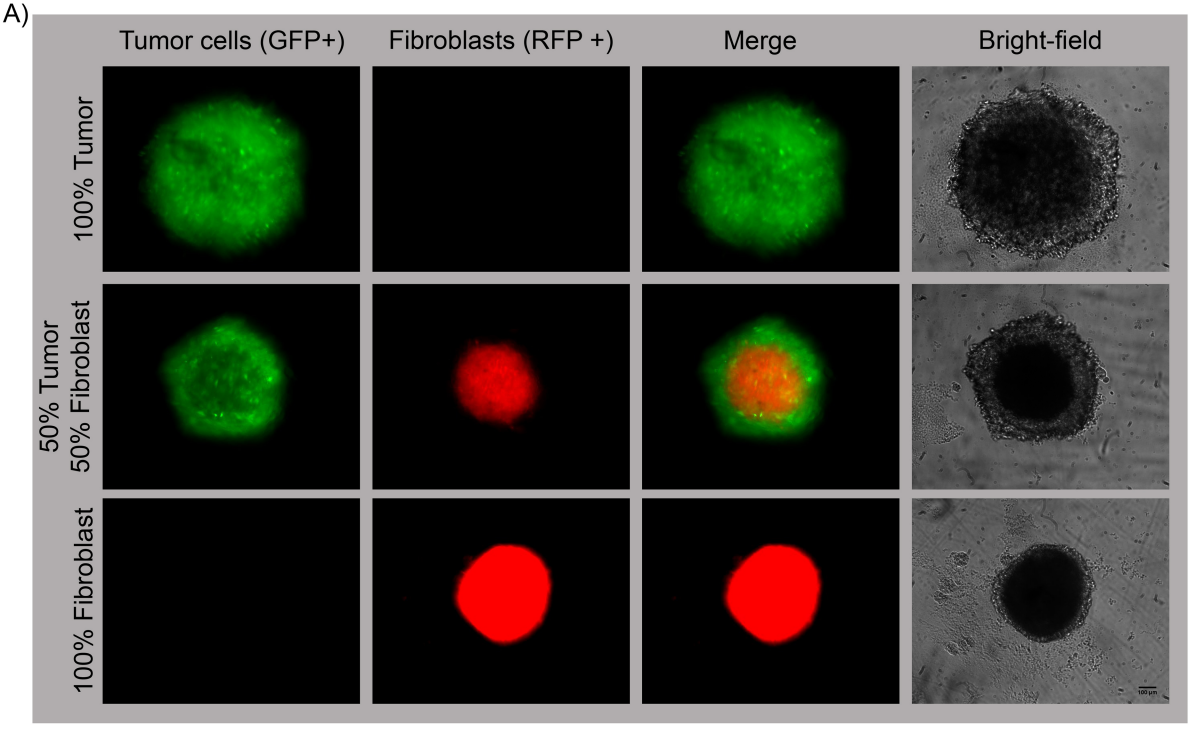
A)
Tumor cells (GFP+)
Fibroblasts (RFP +)
Merge
Bright-field
100% Tumor
50% Tumor
50% Fibroblast
100% Fibroblast

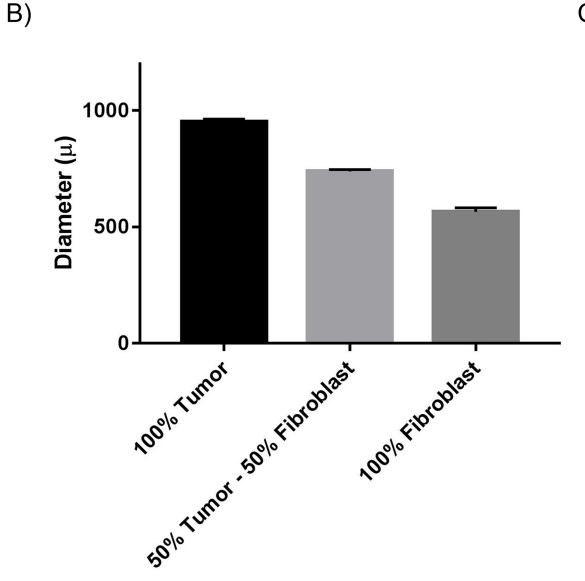
B)
Diameter (μ)
1000
500
0
100% Tumor
50% Tumor - 50% Fibroblast
100% Fibroblast

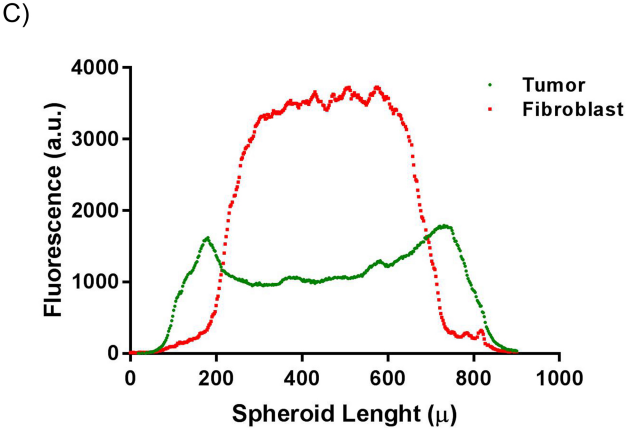
C)
Fluorescence (a.u.)
4000
3000
2000
1000
0
0
200
400
600
800
1000
Spheroid Lenght (μ)
Tumor
Fibroblast

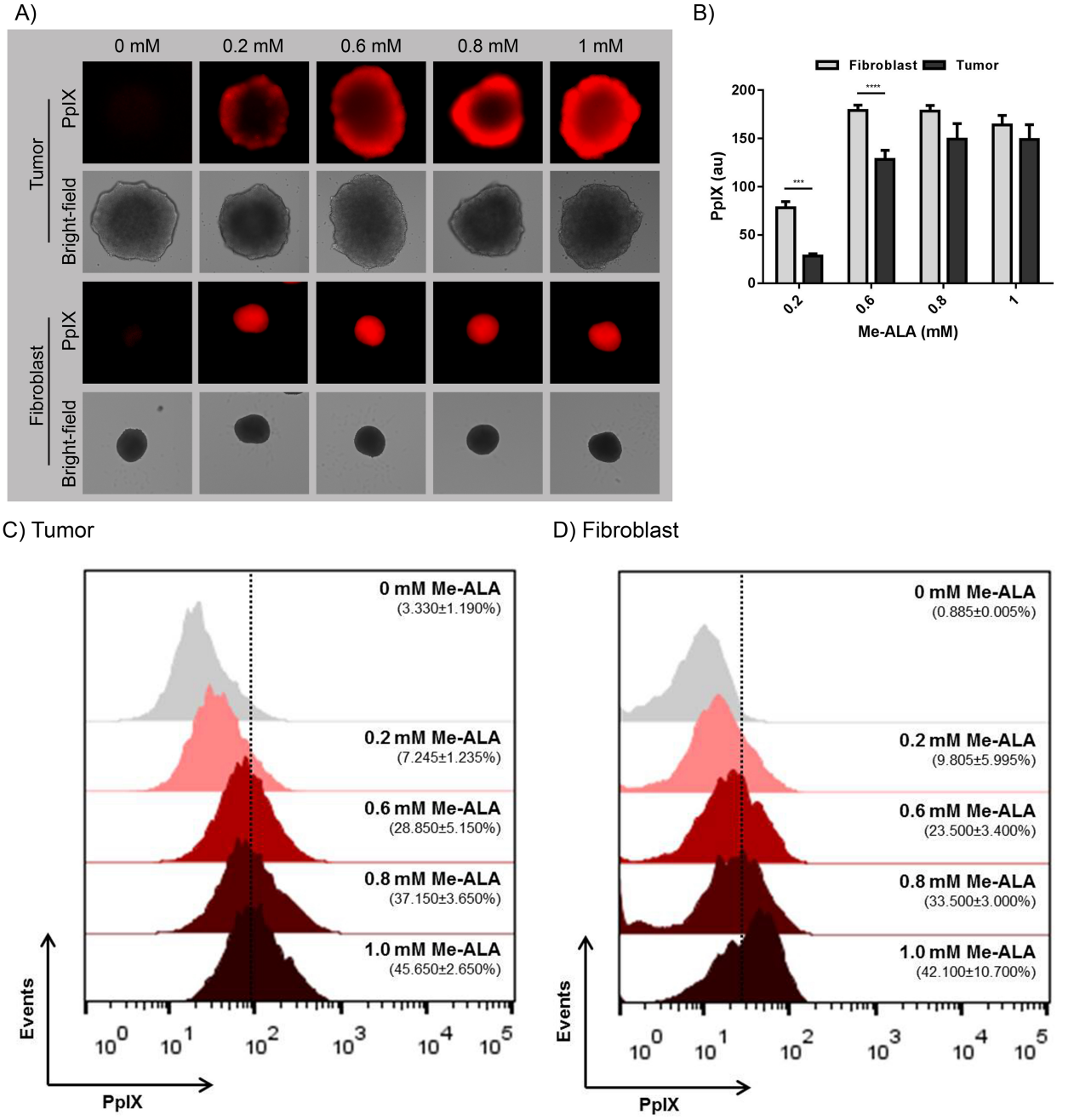
A)
0 mM
0.2 mM
0.6 mM
0.8 mM
1 mM
Tumor
PpIX
Bright-field
Fibroblast
PpIX
Bright-field
B)
Fibroblast
Tumor
PpIX (au)
200
150
100
50
0
***
****
0.2
0.6
0.8
1
Me-ALA (mM)
C) Tumor
0 mM Me-ALA
(3.330±1.190%)
0.2 mM Me-ALA
(7.245±1.235%)
0.6 mM Me-ALA
(28.850±5.150%)
0.8 mM Me-ALA
(37.150±3.650%)
1.0 mM Me-ALA
(45.650±2.650%)
Events
PpIX
D) Fibroblast
0 mM Me-ALA
(0.885±0.005%)
0.2 mM Me-ALA
(9.805±5.995%)
0.6 mM Me-ALA
(23.500±3.400%)
0.8 mM Me-ALA
(33.500±3.000%)
1.0 mM Me-ALA
(42.100±10.700%)
Events
PpIX

A)

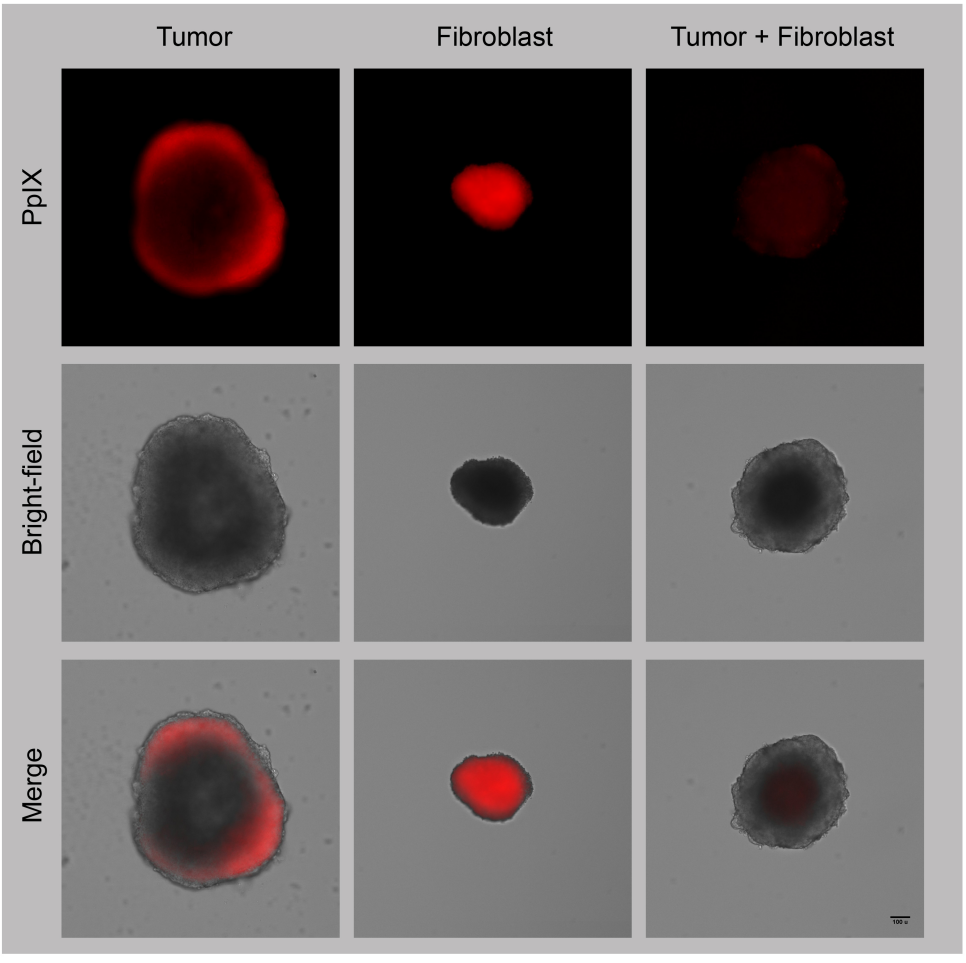
Tumor
Fibroblast
Tumor + Fibroblast
PpIX
Bright-field
Merge

B)

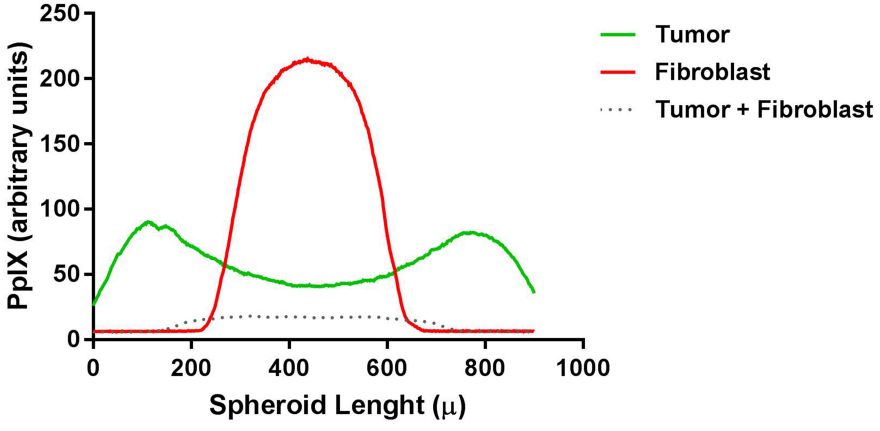
PpIX (arbitrary units)
250
200
150
100
50
0
0
200
400
600
800
1000
Spheroid Lenght (μ)
Tumor
Fibroblast
Tumor + Fibroblast

C)

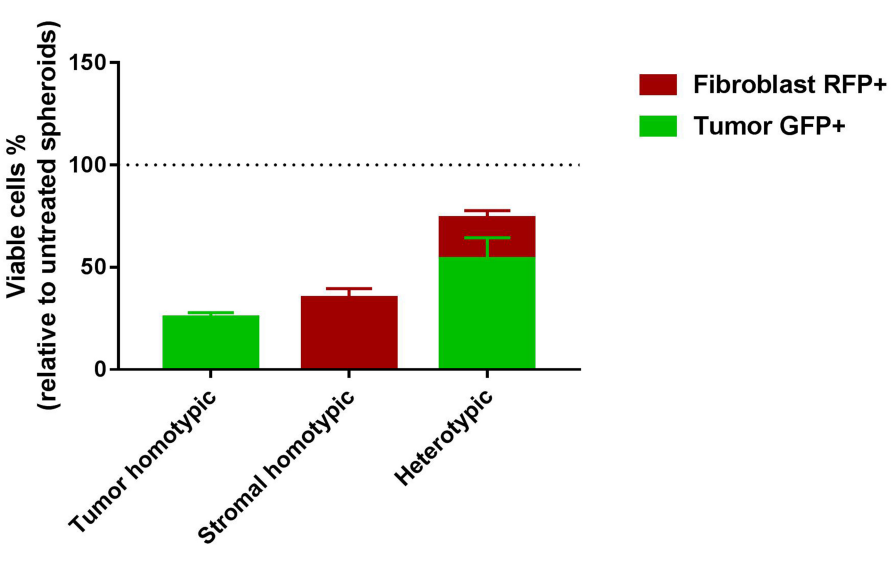
Viable cells %
(relative to untreated spheroids)
150
100
50
0
Tumor homotypic
Stromal homotypic
Heterotypic
Fibroblast RFP+
Tumor GFP+